HiSST: 3rd International Conference on
High-Speed Vehicle Science Technology
14 -19 April 2024, Busan, Korea

Fluid and heat transfer coupled analysis of a hypersonic aircraft with TBCC engine

A. Kikui[1], A. Matsuo[2], E. Shima[3], H. Takahashi[4], H. Taguchi[5], S. Imamura[6]

Abstract

This study evaluated thermal effects on a vehicle airframe of a hypersonic aircraft with a turbine-based combined-cycle (TBCC) engine. The purpose of this study is to evaluate the thermal resistance of the airframe by conducting a coupled thermal-fluid analysis of the airframe geometry designed from an aerodynamic point of view. First, a steady-state fluid analysis was performed on the vehicle airframe to confirm the flow field characteristics, such as shock waves generated from the vehicle nose tip. The flow on the upper surface of the aircraft was accelerated by expansion waves. emanating due to the geometry of the airframe. In the lower part of the aircraft, compression waves were generated from the fuselage-engine joints, and a high pressure area was formed over the intake. In the rear of the engine, the flow was accelerated by the expanding external nozzle. Second, a coupled fluid/heat transfer analysis was performed on the aircraft model. There were temperature vibrations in each case.

Keywords: *Hypersonic Aircraft, Aerodynamic Heating, Hypersonic, CFD*

Nomenclature

Latin
E – Inviscid flux vector in x direction
E_v – Viscos flux vector in x direction
e – Total energy, J/m^3
F – Inviscid flux vector in y direction
F_v – Viscos flux vector in y direction
G – Inviscid flux vector in z direction
G_v – Viscos flux vector in z direction
h – Specific enthalpy, J/kg
K – Thermal conductivity, W / (m・K)
P – Pressure, Pa
Q – conserved-quantity vector
T – Temperature, K
t – Time, s
u – Velocity in x direction
v – Velocity in y direction
w – Velocity in z direction

Greek
β – Thermal diffusion and heat conduction terms
ρ – Density, kg/m^3
τ – Shear stress, Pa

Subscripts
i – Chemical species
S – Solid

[1] *Keio University, 3-14-1 Hiyoshi, Kohoku, Yokohama, Kanagawa, aotok1230@keio.jp*
[2] *Keio University, 3-14-1 Hiyoshi, Kohoku, Yokohama, matsuo@mech.keio.ac.jp*
[3] *Keio University, 3-14-1 Hiyoshi, Kohoku, Yokohama, shima.eiji@jaxa.jp*
[4] *Japan Aerospace Exploration Agency, 7-44-1 Jindaiji-Higashi, Chofu, takahashi.hidemi@jaxa.jp*
[5] *Japan Aerospace Exploration Agency, 7-44-1 Jindaiji-Higashi, Chofu, taguchi.hideyuki@jaxa.jp*
[6] *Japan Aerospace Exploration Agency, 7-44-1 Jindaiji-Higashi, Chofu, imamura.shunsuke@jaxa.jp*

1. Introduction

Japan Aerospace Exploration Agency (JAXA) has proposed a future space transportation system using a winged space vehicle equipped with an air breathing engine[1]. As shown in Fig. 1, the proposed hypersonic aircraft can be used for a space transportation system as a winged booster (first stage high-speed aircraft). After accelerating to a predetermined speed, the booster can launch the upper stage rocket which can travel to the orbit and lands horizontally on the airfield. This allows the booster section to be reused. In this configuration, engines with higher specific impulse than rocket engines, such as air breathing engines, can be used because the booster flies in the atmosphere. Furthermore, the booster can be operated as a high-speed transport between two points on earth.

The proposed winged space vehicle must be capable of accelerating from the still to Mach 6 or 10 using its own engines. In the turbojet engines used in conventional aircraft, thrust is obtained by compressing incoming air to the engine front using a compressor and spraying fuel for combustion. Although the turbojet engine can operate from a standstill, it is difficult to fly above Mach 3 because the air sucked into the engine becomes so hot at high aircraft speeds that the compressor cannot withstand the aerodynamic heating and therefore the engine is damaged. Ramjet and scramjet engines are also capable of hypersonic propulsion, but they cannot operate at standstill and subsonic speeds because they need to compress air to sufficient stat for combusion without using a mechanical turbine. These factors make it difficult to use a single engine to cover the speed range required for space vehicles. For this reason, combined-cycle engines that use different engines depending on the Mach number are considered.

JAXA is considering installing Turbine-Based-Combined-Cycle (TBCC) engines on winged space vehicles. The TBCC engine is a combination of a turbo-ramjet engine and a scramjet engine. TBCC engines are configured with air breathing engines, eliminating the need for an oxidizer onboard the vehicle and so reducing the airframe weight. Turbojet engines are also more reliable than rocket engines.

One of the challenges in realizing a hypersonic aircraft is the problem caused by aerodynamic heating. In addition to the high total temperature due to the high Mach number, there are concerns about heating due to shock wave interference to the airframe. Since the aircraft is also designed to operate as a high-speed point to point transport, it is necessary to check the heat transfer characteristics not only the surface of the aircraft but also inside of the aircraft. Dechaumphai et al.[2] performed numerical analysis of oblique shock waves impinging on a blunt body, and showed that the leading edge of a hypersonic aircraft becomes a stagnation point and causes severe heating, which poses a challenge to the design of the airframe. Liechty et al.[3] measured aerodynamic heating in a Mach 6 wind tunnel for

Fig. 1 Concept of hypersonic aircraft [1]

a booster and a blunt body simulating an orbiter, and showed that the shock wave interaction produced 13 times more heating in the orbiter and 6 times more heating in the booster compared to the single case. However, the insights of heat transfer effects from the airflow to the inside of the fuselage needs to be deepened.

The purpose of this study is to evaluate the thermal resistance of an aircraft designed from aerodynamic viewpoint by conducting a coupled fluid/heat transfer analysis. This report describes the results of the analysis of heat transfer to the airframe using the coupled fluid/heat transfer analysis.

2. Numerical setup

2.1. Governing equations for the calculation

In this report, the three-dimensional compressible Navier-Stokes equations shown in Eq. 1 are used as the governing equations for the fluid analysis, and nitrogen and oxygen are considered as gas species to simulate air. Numerical flux of the convective term is obtained by 2nd order SLAU2[4] with UMUSCL method[5]. The 2nd order central differential scheme is used to discretize the viscous term. LU–SGS implicit method[6] is used for time integration. The *k-ω* model[7] was used for the turbulence model. In addition, ideal gas law shown in Eq. 3 is used to close the system and thermally perfect gas is assumed in this calculation. The thermodynamic characteristic quantities were calculated using the NASA polynomials[8] shown in Eqs. 5 and 6. Heat transfer analysis is calculated by three-dimensional unsteady heat transfer equation shown in Eq. 7. The central difference method was used for discretization and the Crank-Nicolson method for time integration.

$$\frac{\partial \mathbf{Q}}{\partial t}+\frac{\partial(\mathbf{E}-\mathbf{E}_v)}{\partial x}+\frac{\partial(\mathbf{F}-\mathbf{F}_v)}{\partial y}+\frac{\partial(\mathbf{G}-\mathbf{G}_v)}{\partial z}=0 \tag{1}$$

$$\mathbf{Q}=\begin{bmatrix}\rho\\ \rho u\\ \rho v\\ \rho w\\ e\\ \rho_i\end{bmatrix},\ \mathbf{E}=\begin{bmatrix}\rho u\\ \rho u^2+p\\ \rho uv\\ \rho uw\\ (e+p)u\\ \rho_i u\end{bmatrix},\mathbf{F}=\begin{bmatrix}\rho v\\ \rho vu\\ \rho v^2+p\\ \rho vw\\ (e+p)v\\ \rho_i v\end{bmatrix},\mathbf{G}=\begin{bmatrix}\rho v\\ \rho wu\\ \rho \mathrm{w}v\\ \rho w^2+p\\ (e+p)w\\ \rho_i w\end{bmatrix},\mathbf{E}_v=\begin{bmatrix}0\\ \tau_{xx}\\ \tau_{yx}\\ \tau_{zx}\\ \beta_x\\ 0\end{bmatrix},\mathbf{F}_v=\begin{bmatrix}0\\ \tau_{xy}\\ \tau_{yy}\\ \tau_{zy}\\ \beta_y\\ 0\end{bmatrix},\mathbf{G}_v=\begin{bmatrix}0\\ \tau_{xz}\\ \tau_{yz}\\ \tau_{zz}\\ \beta_z\\ 0\end{bmatrix} \tag{2}$$

$$\tau_{xx}=\frac{2}{3}\mu\left(2\frac{\partial u}{\partial x}-\frac{\partial v}{\partial y}-\frac{\partial w}{\partial z}\right)$$

$$\tau_{yy}=\frac{2}{3}\mu\left(2\frac{\partial v}{\partial y}-\frac{\partial u}{\partial x}-\frac{\partial w}{\partial z}\right)$$

$$\tau_{zz}=\frac{2}{3}\mu\left(2\frac{\partial w}{\partial z}-\frac{\partial u}{\partial x}-\frac{\partial v}{\partial y}\right)$$

$$\tau_{xy}=\tau_{yx}=\mu\left(\frac{\partial u}{\partial y}+\frac{\partial v}{\partial x}\right)$$

$$\tau_{yz}=\tau_{zy}=\mu\left(\frac{\partial v}{\partial z}+\frac{\partial w}{\partial y}\right)$$

$$\tau_{zx}=\tau_{xz}=\mu\left(\frac{\partial w}{\partial x}+\frac{\partial u}{\partial z}\right)$$

$$\rho=\sum_i \rho_i$$

$$e=\sum_i \rho_i h_i-p+\frac{\rho}{2}(u^2+v^2+w^2)$$

$$\beta_x=u\tau_{xx}+v\tau_{xy}+w\tau_{xz}-q_x$$

$$\beta_y=u\tau_{yx}+v\tau_{yy}+w\tau_{yz}-q_y$$

$$\beta_z=u\tau_{zx}+v\tau_{zy}+w\tau_{zz}-q_z$$

$$q_x = -\kappa\frac{\partial T}{\partial x} - \rho\sum_{i=1}^{N} h_i D_i \frac{\partial Y_i}{\partial x}$$

$$q_y = -\kappa\frac{\partial T}{\partial y} - \rho\sum_{i=1}^{N} h_i D_i \frac{\partial Y_i}{\partial y}$$

$$q_z = -\kappa\frac{\partial T}{\partial z} - \rho\sum_{i=1}^{N} h_i D_i \frac{\partial Y_i}{\partial z}$$

$$p = \rho RT \tag{4}$$

$$\frac{h}{RT} = a_1 + \frac{a_2 T}{2} + \frac{a_3 T^2}{3} + \frac{a_4 T^3}{4} + \frac{a_5 T^4}{5} + \frac{b}{T} \tag{5}$$

$$\frac{C_p}{R} = a_1 + a_2 T + a_3 T^2 + a_4 T^3 + a_5 T^4 \tag{6}$$

$$\rho_s \frac{\partial h_s}{\partial t} = \frac{\partial}{\partial x}\cdot\left(\kappa_s \frac{\partial T}{\partial x}\right) + \frac{\partial}{\partial y}\cdot\left(\kappa_s \frac{\partial T}{\partial y}\right) + \frac{\partial}{\partial z}\cdot\left(\kappa_s \frac{\partial T}{\partial z}\right) \tag{7}$$

2.2. Fluid-Thermal Coupled Analysis Method

A loosely coupled method[9] was used to couple the fluid analysis with heat transfer in solids. This method assumes that the flow field converges much faster than transitional heat transfer. From this assumption, the fluid can be assumed to reach a steady state instantaneously. Therefore, the time evolution of the solid temperature is obtained by repeating the steady-state calculation for the fluid and the heat transfer calculation for the solid.

Fig. 2 illustrates the procedure of the loosely coupled method, and its detail is as follows. First, initial wall temperature of the solid is set. Next the solid wall temperature is set to the isothermal wall temperature of the fluid steady-state analysis. Then, fluid steady-state analysis is performed and the heat flux distribution is set as the initial condition for heat transfer analysis. Heat transfer analysis is then performed for a coupling time interval. At this time, the fluid side is not calculated. The wall surface temperature obtained from the heat transfer analysis is set as the new isothermal wall temperature, and the fluid steady-state analysis is performed. This procedure was repeated for the coupled analysis. In this report, the coupling time interval is 5.0 s.

2.3. Analysis target

The analysis target is shown in Fig. 3. The aircraft is 50 m long and 40 m wide. The material of the body is titanium alloy. A TBCC engine is attached to the lower part of the body. The total number of

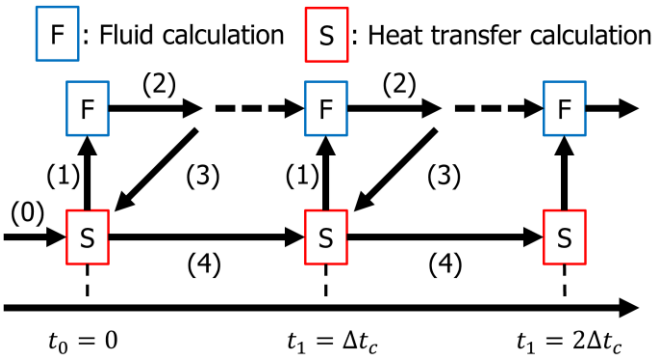

Fig. 2 The procedure of loosely coupled method

cells is 2400000. The minimum grid width in the nomall to the fuselage wall in the fluid analysis was set to 2 μm and to capture the boundary layer, the grid near the wall surface is finer. This calculation does not reproduce the flow path of the turbojet and does not deal with combustion. The Mach number of the mainstream is 5.28, the static pressure is 1.79 kPa, and the static temperature is 223 K. The initial temperature of the airframe is 298.15 K. The angle of attack is 6.78 deg. This simulates the flight conditions of this aircraft in cruise.

3. Results

3.1. Steady-state fluid analysis with adiabatic walls

To investigate the flow characteristics around the aircraft, a steady-state analysis of the fluid flow with the aircraft wall as an adiabatic wall was performed before the coupled analysis. In this case, the solid interior of the airframe is not calculated. The wall surface temperature obtained by steady-state analysis using an adiabatic wall indicates the temperature of the fluid near the wall surface, which is the state in which heat conduction to the solid has reached steady-state and the temperature of the aircraft wall surface is the same as the fluid temperature. Therefore, the results of the steady-state analysis with the adiabatic wall serve as an indicator to confirm the temperature distribution on the aircraft surface as the coupled analysis proceeds and the steady-state condition is approached. On the other hand, the temperature gradient inside the solid is not reproduced, so it does not match the actual value.
Fig. 4 shows the Mach number distribution in the fluid steady state solution. Fig. 4 shows that the flow is accelerated by expansion waves from the tip of the aircraft to the top of the aircraft and decelerated by shock waves generated from the tip of the aircraft and from the junction between the fuselage and the engine because the nose of the plane is set at an angle of attack of 6.78 deg. The nozzle behind the engine was enlarged and the flow was accelerated. The analysis condition simulates cruise condition and are not the design point of the aircraft. Therefore, shock waves generated from the aircraft tip do not attach to the tip of the scramjet engine intake.
Fig. 5 shows the temperature distribution on the lower part of the fuselage and wing surfaces. In the geometry analyzed in this study, the stagnation points appear at the leading edge of the aircraft, the connection between the engine and the fuselage, and the intake cowl. A high temperature region at the tip was observed flowing downstream, and the temperature at the tip was 1327 K. The temperature at the junction of the aircraft and the engine was 1358 K, which was higher than that at the tip of the aircraft. Smoother connection between fuselage and engine is needed to avoid high temperatures. A hot region was generated on the sidewall of the intake, and the hot region was observed to flow into the rear intake and out of the intake. This is believed to be due to the generation of shock waves from the sidewalls of the intakes, which interfered with the shock waves and caused the temperature to rise over a wide area.

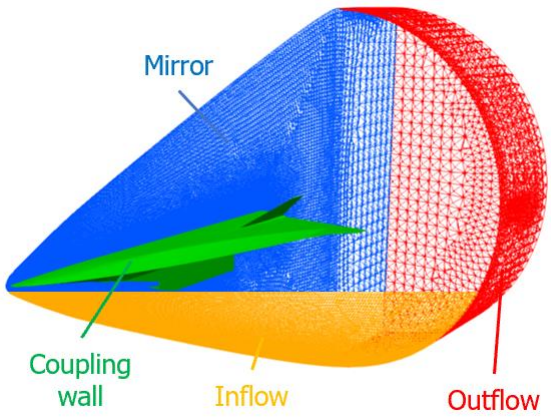

Fig. 3 Grid for analysis

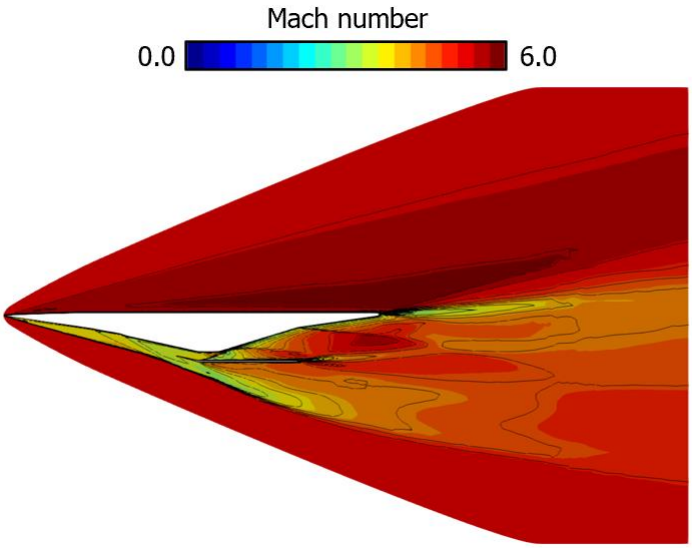

Fig. 4 Mach number distribution in steady state

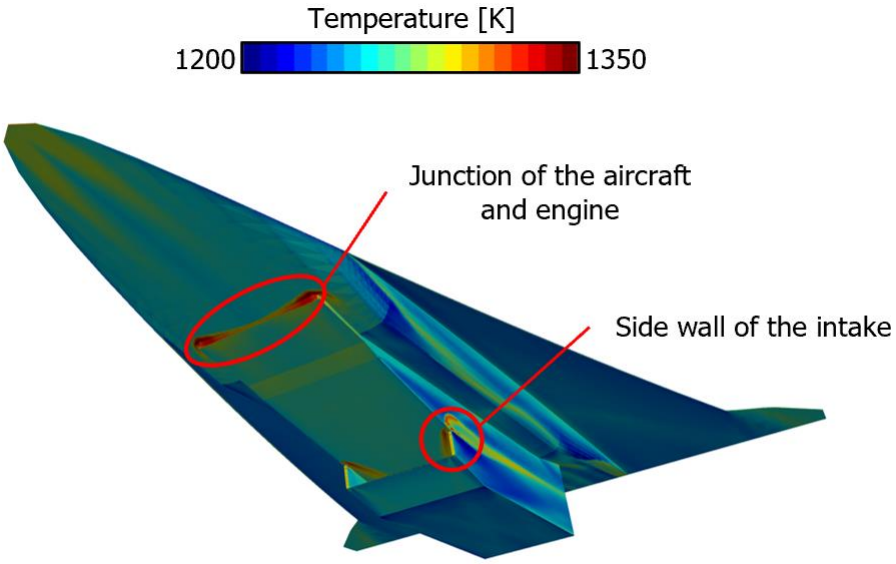

Fig. 5 Temperature distribution on the fuselage surface obtained by steady-state analysis with adiabatic walls

3.2. Steady-state fluid analysis with isothermal walls

To obtain the initial conditions for the coupled fluid-solid heat transfer analysis, a steady-state analysis of the fluid was performed with the fuselage wall as an isothermal wall. Heat transfer calculations inside the fuselage are not performed as aforementioned. Fig. 6 shows the heat flux distribution under steady state conditions. The heat flux was less than 300 kW/m^2 in most areas, but exceeded 1000 kW/m^2 at the tip of the aircraft, at the fuselage-engine junction, and at the intake. Therefore, the coupled analysis may result in higher temperatures at these three points.

3.3. Coupled analysis

The coupled fluid-solid heat transfer calculations were performed using the results of the fluid steady-state analysis performed in the previous section, in which the aircraft wall was assumed to be an isothermal wall, as the initial condition.

Fig. 7 shows the temperature distribution on the aircraft wall at t=240 s after the start of the coupled analysis. The lower surface of the aircraft has, in general, higher temperature than the upper surface.

This is due to the shock wave generated in the lower area of the aircraft as air flows from below due to the angle of attack on the main stream. On the top surface of the aircraft, the temperature rose to 700 K at the sloping edge of the wing, but fell below 400 K in the other areas. On the underside of the aircraft, the temperature rose to 1100 K at the stagnant points: the tip of the aircraft, the junction between the aircraft and the engine, and the cowl of the intake. The reason for the higher cowl temperature is thought to be that the cowl is thin and has a large surface area and small volume, resulting in a larger temperature increase even when the added heat flux is less than the stagnation point. High-temperature areas were also observed near the tip of the aircraft and in the sloping areas near the wings. The cause is thought to be adiabatic compression of the fluid due to the increased angle of the wall surface to the flow.

Fig. 8 shows the temperature history of the tip of the aircraft, the junction of the aircraft and engine, and the cowl of the intake. The figure indicates that the temperature rise processes in the three locations were almost the same. Therefore, if the maximum temperature is calculated in the analysis of a simple model, the results can be applied to complex geometries. However, there were temperature vibrations in each case.

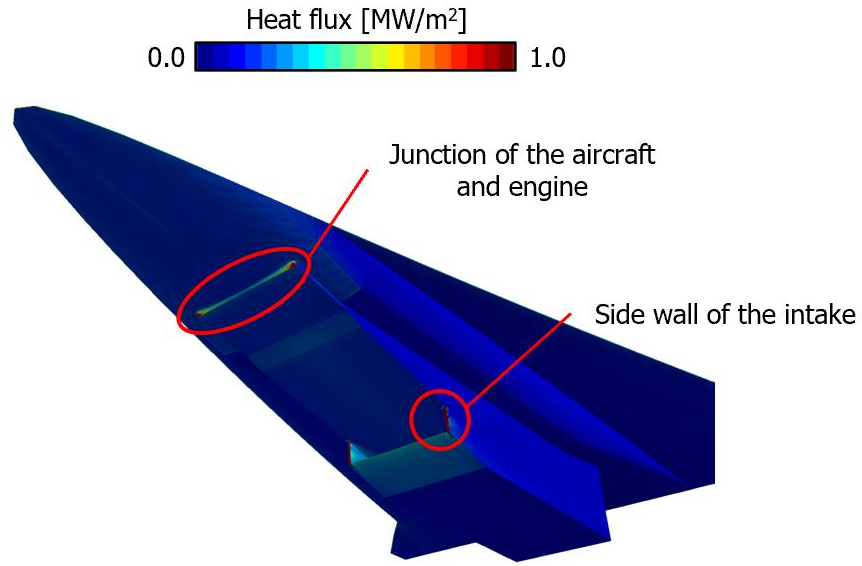

Fig. 6 Heat flux distribution on the aircraft in steady state

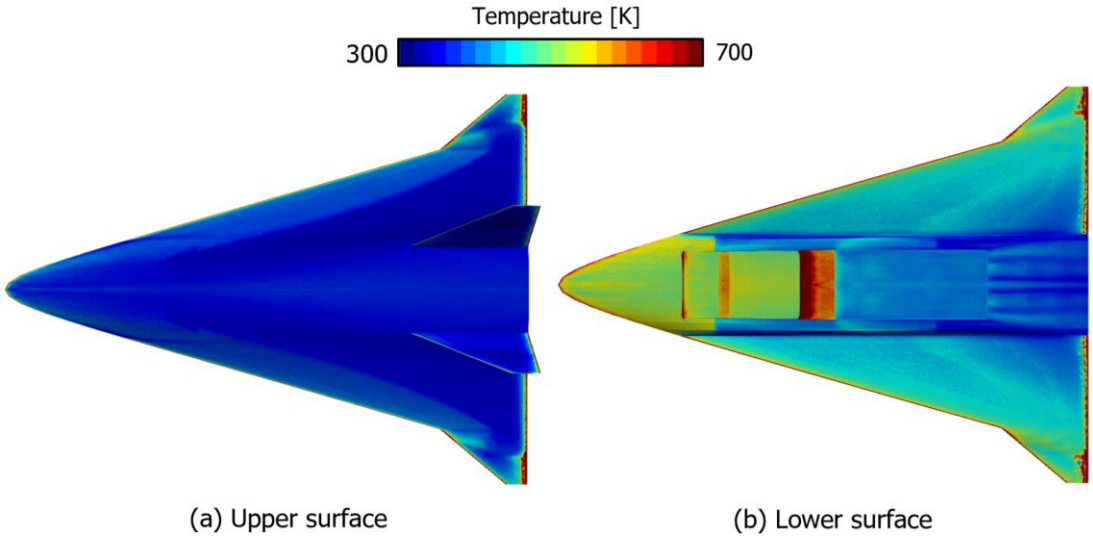

Fig. 7 Temperature distribution on the aircraft wall at t=240 s

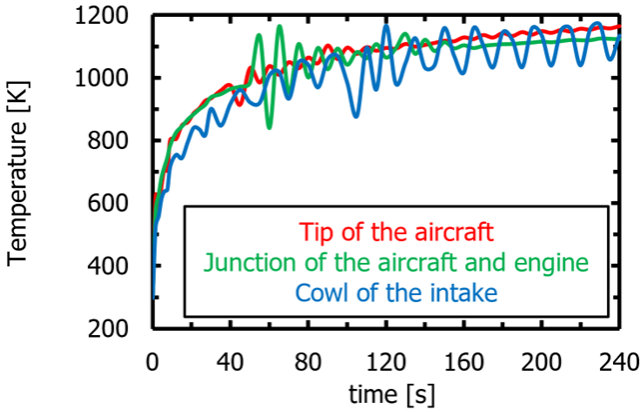

Fig. 8 Temperature history at stagnation point

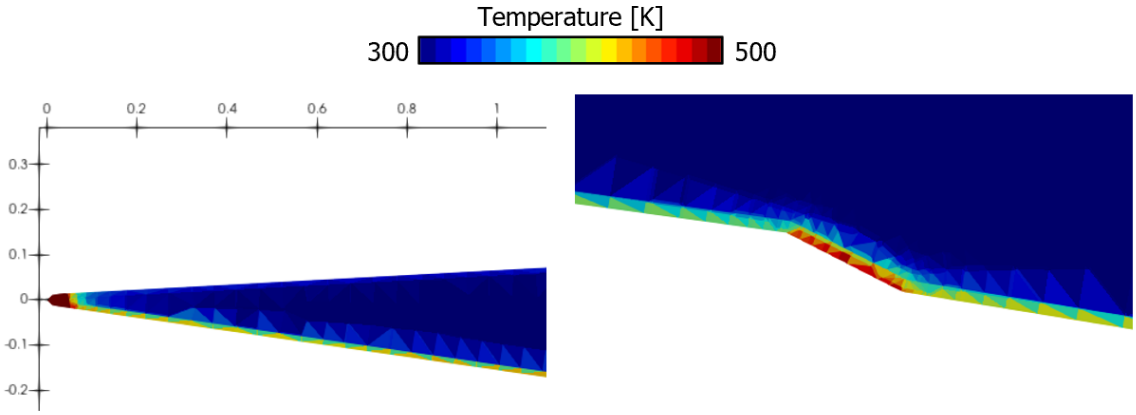

(a) Tip of the aircraft (b) Junction of the aircraft and engine

Fig. 9 Temperature distribution inside the aircraft at t=240 s

Fig. 9 shows the temperature distribution inside the aircraft at t = 240 s. At the tip of the aircraft, heat is transferred from the tip to about 0.4 m. At the junction of the fuselage and engine, heat is transferred to about 0.04 m from the aircraft wall. At the aircraft-engine junction, heat is transferred up to about 0.04 m from the aircraft wall. In addition, because the analysis in this report assumes the interior of the aircraft to be a solid metal, temperatures do not increase in almost all areas of the aircraft interior. This analysis was conducted with a solid model to confirm the calculation method. Detailed analyses with a real structure will be conducted in the next step.

4. Conclusion

In this study, an aerodynamic heating analysis of a proposed hypersonic aircraft model was performed with a simple solid model. The temperature field on the airframe and engine surfaces and temperature history at the stagnation point was obtained. In the future, it will be necessary to perform calculations for longer timespan with a detailed internal structure in order to determine the temperature distribution inside the aircraft accounting for a flight demonstration.

References

1. Taguchi, H., Futamura, H., Yanagi, R. and Maita, M.: Analytical Study of Pre-Cooled Turbojet Engine for TSTO Spaceplane. 10th AIAA/NAL-NASDA-ISAS International Space Planes and Hypersonic Systems and Technologies Conference, 2001-1838 (2001)

2. Dechaumphai, P., Thornton, Earl A. and Wieting, Allan R.: Flow-Thermal-Structural Study of Aerodynamically Heated Leading Edges. Journal of Spacecraft and Rockets. 26, 201-288 (1989)
3. Liechty, D. S.: Aeroheating Characteristics for a Two-Stage-To-Orbit Concept During Separation at Mach 6. 35th AIAA FluidDynamics Conference and Exhibit, AIAA2005-5139 (2005)
4. Kitamura, K. and Shima, E.: Towards shock-stable and accurate hypersonic heating computations: A new pressure flux for AUSM-family schemes. Journal of Computational Physics. 245, 62-83 (2013)
5. Burg, C. O. E.: Higher order variable extrapolation for unstructured finite volume RANS flow solvers, 17th AIAA Computational Fluid Dynamics Conference, pp.1–17 (2005)
6. Sharov, D. and Nakahashi, K.: Reordering of 3-D Hybrid Unstructured Grids for Vectorized LU-SGS Navier-Stokes Computations. 13th Computational Fluid Dynamics Conference. 97-2102 (1997)
7. Wilcox, D. C.: Turbulence Modeling for CFD, DCW Industries (2006)
8. Svehla, Roger A.: Estimated viscosities and thermal conductivities of gases at high temperature (1962)
9. Chen, F., Liu, H. and Zhang, S.: Time-adaptive loosely coupled analysis on fluid–thermal–structural behaviors of hypersonic wing structures under sustained aeroheating. Aerospace Science and Technology.78, 620-636 (2018)